Earth and Planetary Science Letters 335–336 (2012) 36–47

Contents lists available at SciVerse ScienceDirect

Earth and Planetary Science Letters

journal homepage: www.elsevier.com/locate/epsl

Coupled basin-detachment systems as paleoaltimetry archives of the western North American Cordillera

Aude Gébelin [a,b,*], Andreas Mulch [b,c,d], Christian Teyssier [e], C. Page Chamberlain [f], Matthew Heizler [g]

[a] Institut für Geologie, Leibniz Universität Hannover, 30167 Hannover, Germany
[b] Biodiversity and Climate Research Centre (BiK-F), Senckenberganlage 25, 60325 Frankfurt/Main, Germany
[c] Institut für Geowissenschaften, Goethe Universität Frankfurt, Altenhöferallee 1, 60438 Frankfurt/Main, Germany
[d] Senckenberg, Senckenberganlage 25, 60325 Frankfurt/Main, Germany
[e] Earth Sciences, University of Minnesota, Minneapolis, MN 55455, USA
[f] Environmental Earth Systems Science, Stanford University, Stanford, CA 94305, USA
[g] Bureau of Geology and Mineral Resources, Socorro, NM 87801, USA

ARTICLE INFO

Article history:
Received 24 November 2011
Received in revised form
18 April 2012
Accepted 20 April 2012
Editor: T.M. Harrison

Keywords:
paleoaltimetry
stable isotope
detachment
Basin
North American Cordillera
Snake Range

ABSTRACT

Stable isotope paleoaltimetry data from the Snake Range metamorphic core complex (MCC) and Sacramento Pass Basin (NV, USA) document that extensional mylonite zones and kinematically linked syntectonic basins reliably record paleotopography in the continental interior of western North America when compared to a sea-level reference. Here we show that this basin–MCC pair tracks meteoric fluid flow at different levels of actively extending crust in a high-topography region during Oligo-Miocene extension of the Basin and Range Province. For paleoaltimetry purposes we compare multi-proxy oxygen ($\delta^{18}O$) and hydrogen (δD) isotope data as well as geochronological information from the Snake Range MCC to a time-equivalent (ca. 20 Ma) stable isotopic proxy record from the Buckskin Mountains MCC (AZ, USA), which developed next to the Pacific Coast near Miocene sea level. We complement this paleoaltimetry study by comparing the Buckskin Mountains MCC data with older ($\sim$35 Ma) lacustrine stable isotope and paleofloral records from the nearby House Range (UT, USA), whose paleoelevation has been determined independently through paleobotanical analysis. Each of the investigated compartments of the paleohydrologic system within the Snake Range MCC depicts a coherent scenario of low Oligo-Miocene $\delta^{18}O$ and δD values of meteoric water that reflect precipitation sourced at high elevation. A 77‰ difference in δD_{water} between the Snake Range ($\delta D_{water} \sim -113$‰) and the Buckskin Mountains ($\delta D_{water} \sim -36$‰) is consistent with minimum mean paleoelevation of the Snake Range of about 3850 ± 650 m above Miocene sea level. Additional support for such elevations comes from a comparison between the Buckskin Mountains MCC and the Eocene House Range basin (UT, USA) where differences in $\delta^{18}O_{water}$ values are consistent with 2300 ± 500 m minimum paleoelevation of the House Range. Based on the presence of brecciated rock-avalanche deposits within the Sacramento Pass Basin, we conclude that the Snake Range was a topographic high and locus of significant relief during regional scale extension within the Cordilleran hinterland.

1. Introduction

The elevation of the Earth's surface is one of the most important characteristics of continental lithosphere and reflects the distribution of mass and heat inside the Earth, controls drainage patterns and detrital recycling, and influences atmospheric circulation and therefore precipitation and climate (e.g. Ruddiman and Kutzbach, 1989; Molnar and England, 1990). During the past decade stable isotope studies have reconstructed the paleoelevation of mountains belts. These studies exploit changes in meteoric water composition preserved in the geologic near surface record, using authigenic minerals from paleosol and paleolake deposits (e.g. Chamberlain et al., 1999; Garzione et al., 2000; Poage and Chamberlain, 2002; Horton et al., 2004; Garzione et al., 2006; Kent-Corson et al., 2006; Mulch et al., 2006, 2008; Rowley and Currie, 2006; Davis et al., 2009; Mix et al., 2011), or in deeper parts of the crust using silicates from extensional shear zones (Mulch et al., 2004, 2007).

The paleotopography of western North America has been a matter of debate, in particular since the advent of quantitative paleoaltimetry methods (e.g. Chamberlain et al., 1999; Poage and

* Corresponding author at: Institut für Geologie, Leibniz Universität Hannover, 30167 Hannover, Germany. Tel.: +49 69 7542 1883; fax: +49 69 7542 1802.
E-mail address: aude.gebelin@senckenberg.de (A. Gébelin).

0012-821X/$ - see front matter © 2012 Elsevier B.V. All rights reserved.
http://dx.doi.org/10.1016/j.epsl.2012.04.029

Chamberlain, 2001; Rowley and Currie, 2006; Rowley and Garzione, 2007). Abundant geologic and geochronologic evidence indicates that Cretaceous to Paleocene crustal shortening produced a welt of thickened continental crust that likely manifested itself in a high continental interior during and after the Sevier orogeny (Nevadaplano, DeCelles et al., 1995; DeCelles, 2004). Early Oligocene high elevations in the Cordilleran hinterland have been taken as evidence that late Mesozoic to early Cenozoic tectonics were responsible for a post-Sevier continental interior highland that subsequently collapsed to modern elevations (Gregory-Wodzicki, 1997; Wolfe et al. 1997; DeCelles, 2004).

Interestingly, a vast body of stable isotope paleoaltimetry data (e.g. Horton et al., 2004; Horton and Chamberlain, 2006; Kent-Corson et al., 2006; Davis et al., 2009; Mix et al., 2011; Chamberlain et al., in press) finds increasing evidence for extended dry continental highlands at about 49 Ma in British Columbia, Washington, and Montana, and ca. 40 Ma in central Nevada. Most of these paleoaltimetry studies use stable isotopic analyses of different terrestrial paleoclimate proxies from all over the orogen (Horton and Chamberlain, 2006; Mix et al., 2011; Chamberlain et al., in press). However, one major concern commonly observed is that each isotopic proxy material (lacustrine, palustrine, or pedogenic carbonates (Quade et al., 2007), authigenic and recrystallized silicates (Mulch and Chamberlain, 2007), or sedimentary or primary organic matter (e.g. Hren et al., 2010)) used as single-site stable isotope paleoaltimetry reconstructions have their individual biases when trying to reconstruct $\delta^{18}O$ or δD of precipitation from their isotopic composition.

Here we extend these approaches by combining multi-proxy, multi-isotope data from extensional mylonite zones and kinematically linked syntectonic basins that record paleotopographic and climatic changes during Cenozoic extension of the western North American Cordillera. We focus on the Snake Range metamorphic core complex (MCC) and Sacramento Pass Basin (NV, USA) (Fig. 1) that co-developed as a consequence of Oligo-Miocene extension of the Basin and Range Province. Collectively, this basin-core complex system provides an excellent opportunity to retrieve stable isotope data from different environments and levels of the crust, and tracks pathways of meteoric fluid flow from the critical zone at the biosphere–geosphere interface to the actively extending middle crust. We compare oxygen ($\delta^{18}O$) and hydrogen (δD) isotope ratios of mineral proxies from the high-topography region of the Snake Range in the continental interior to syntectonic minerals that crystallized at ~20 Ma during detachment activity of the Buckskin Mountains MCC (AZ, USA, Fig.1) that at the time was located close to the Pacific Coast near Miocene sea level.

The Snake Range and Buckskin Mountains represent classic examples of normal fault-bounded MCC. Even though detachments in both MCC are similar in age and in their role in shaping and

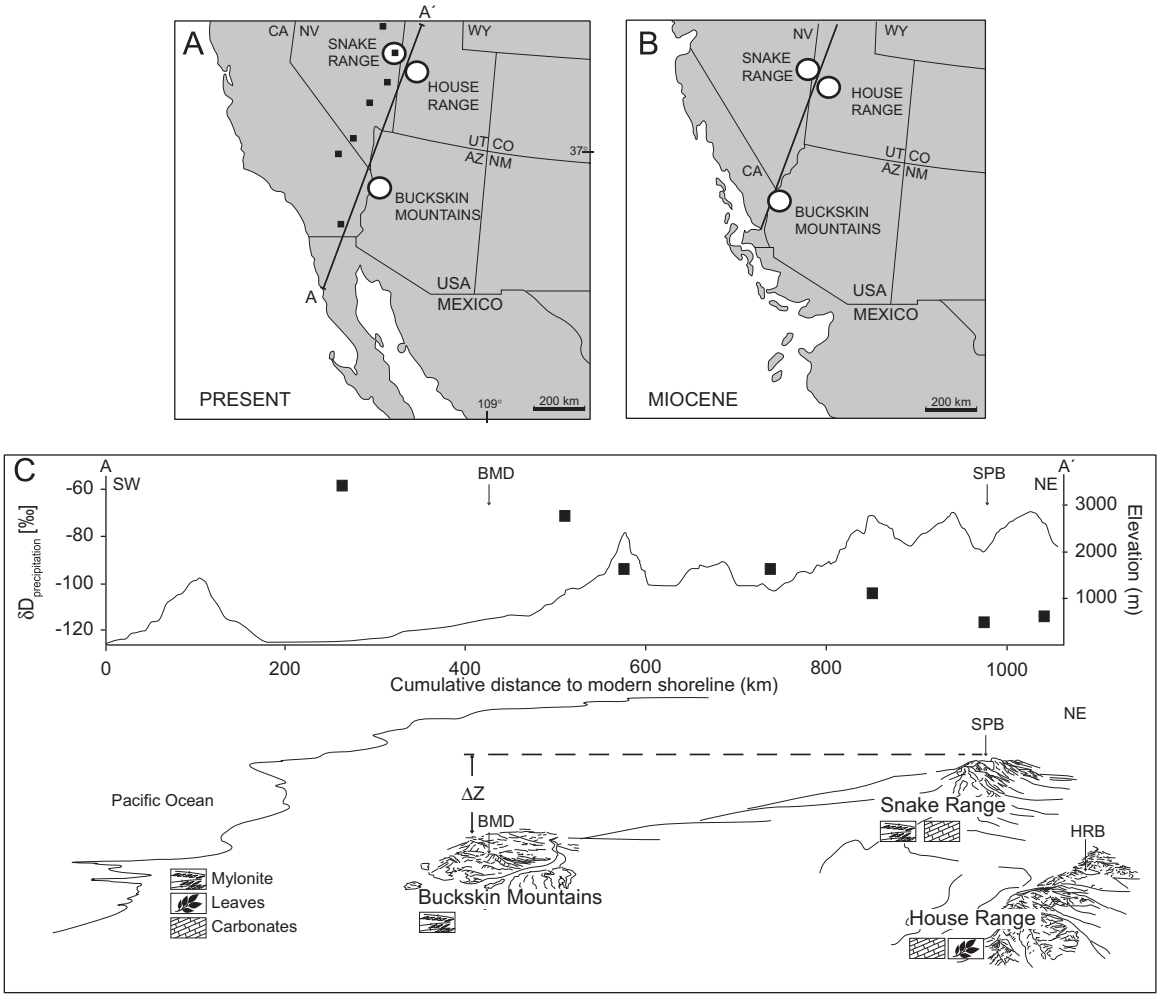

Fig. 1. Present-day (A) and Miocene Paleogeographic (B) Basin and Range Maps (after Blakey, 2011) showing position of the Snake Range, House Range, and Buckskin Mountains. Black dots in (A) are monitoring sites for isotopes in precipitation (Friedman et al., 2002b); corresponding $\delta D_{precipitation}$ values are shown in (C). (C) Present location of the Buckskin Mountains, Snake Range, and House Range along a NE–SW transect in the Basin and Range Province and their correlation with $\delta D_{precipitation}$. The black line indicates the topographic profile across the three different areas. BMD, Buckskin Mountains Detachment; SPB, Sacramento Pass Basin; HRB, House Range basin.

transforming the extending Cordilleran orogen, stable isotope data suggest that meteoric fluids that entered these two detachments had vastly different isotopic compositions. Therefore, $\delta^{18}O$ and δD values of precipitation (as the ultimate source for the meteoric water) in central Nevada must have been affected by different atmospheric circulation conditions including, but not limited to, higher surface elevations and increased continentality. We further complement our results by comparing the Buckskin Mountains isotope data to a slightly older (~35 Ma) lacustrine stable isotope record from the nearby House Range (UT, USA, Fig.1). Here, paleoelevation estimates of 2.9 ± 1.5 to 3.6 ± 0.7 km have been determined independently through paleobotanical analysis (Gregory-Wodzicki, 1997).

Our alternative approach to determining paleoelevation relies on a comparison of high-elevation multi-proxy stable isotope records from the continental interior to near-sea level records to reduce potential biases on stable isotope in precipitation patterns (e.g. Mulch et al., 2006) that may be due to paleoclimate change. Each of the investigated compartments of the paleohydrologic

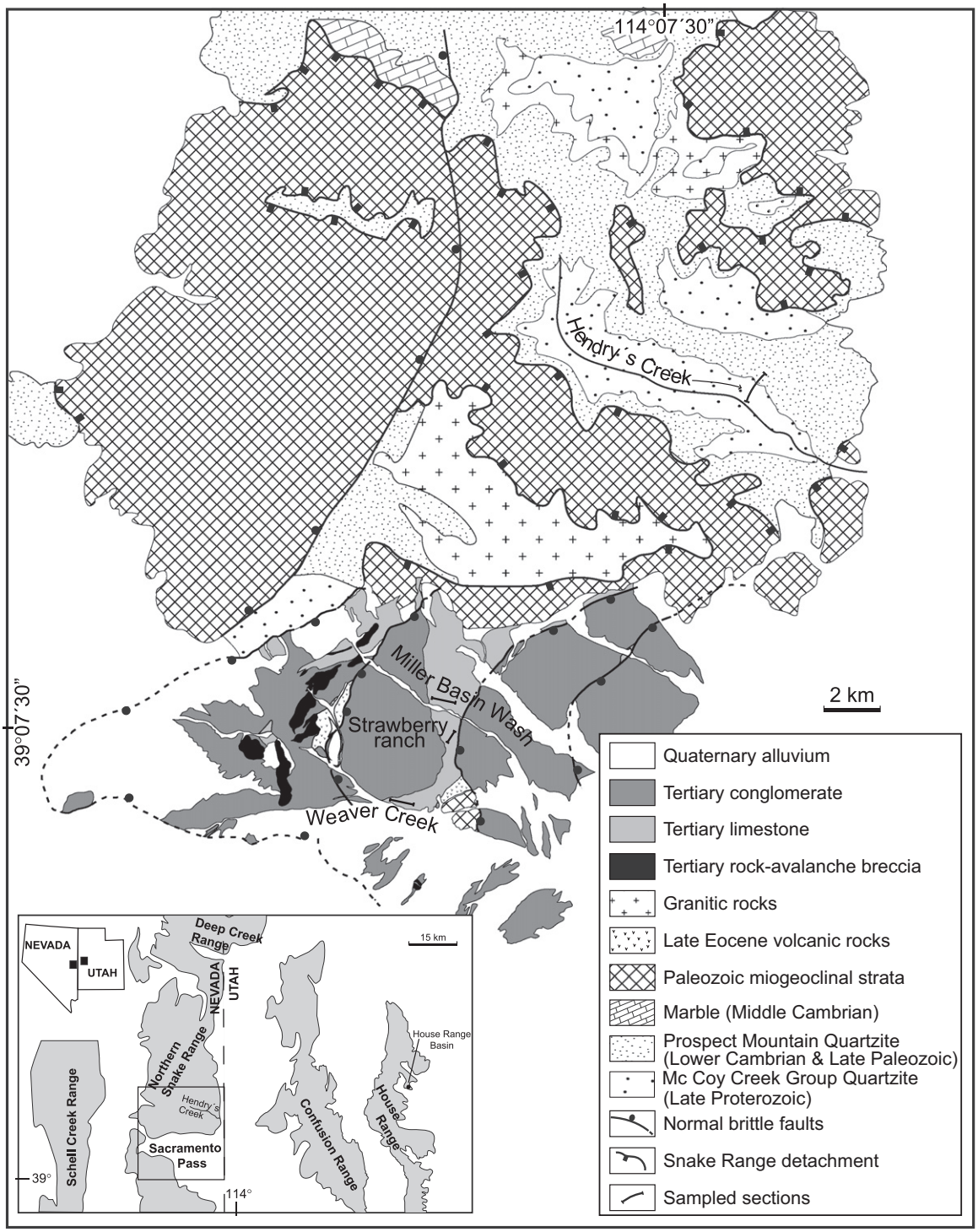

Fig. 2. Geological map of the southeastern corner of the Northern Snake Range and the Sacramento Pass Basin. Solid transect lines represent sub-sections through the lacustrine deposits of the Sacramento Pass Basin and detachment footwall at Hendry's Creek.

system that cover various levels of continental crust (lacustrine sediments, hanging wall brittle faults, footwall mylonite) in the Snake Range MCC depicts a coherent scenario of low (Oligo-Miocene) meteoric $\delta^{18}O_{water}$ and δD_{water}. Comparison with δD_{water} from mylonitic quartzite of the Buckskin Mountains MCC (AZ, USA) shows that meteoric water in the Snake Range originated at high elevations ($\sim 3850 \pm 650$ m) in an area with strong relief. As such we suggest that the Oligo-Miocene Snake Range was part of a topographic high within the Cordilleran hinterland.

2. Northern Snake Range

The Northern Snake Range MCC experienced rapid Oligo-Miocene exhumation and extensional faulting and exposes a 150 km N–S-trending low angle detachment overlain by Miocene sediments of the Sacramento Pass supradetachment basin (SPB) (Grier, 1984; Martinez, 1999; Miller et al., 1999a, 1999b) (Fig. 2). With a top to the east sense of shearing, the Northern Snake Range Detachment (NSRD) accommodated exhumation of Precambrian and Cambrian quartzite relative to upper plate Paleozoic units (Wernicke, 1981; Lee et al., 1987; Miller et al., 1999a) and exposes an almost complete footwall-hanging wall cross section of muscovite-bearing quartzite mylonite and schist at Hendry's Creek (Figs. 2 and 3; see detailed description of the sampled cross section in Gébelin et al., 2011).

Sediments in the SPB include playa lake facies of conglomerate and lacustrine limestone interfingered with brecciated Paleozoic rock-avalanche deposits. These deposits record changing depositional environments in the SPB that were governed by changes in paleohydrology and relief in the basin drainage (Grier, 1984; Fig. 2). Lacustrine carbonates from three localities (Miller Basin Wash, MBW; Weaver Creek, WC; and Strawberry Ranch, SR) form a ca. 120 m thick composite stratigraphic section through the SPB (Figs. 2 and 3). They consist of yellow to tan limestone beds that vary in thickness from 2 cm to 3 m. Micrite and sparite are the main components with additional allochemical clasts, terrigenous detritus, anhydrite, and gypsum. Sparite only appears surrounding clasts, or as blocky sparite fillings (Grier, 1984). Both types of cement indicate a fresh water environment (Folk, 1974) but the stable isotope data presented here was obtained from the micrite component, only. These lacustrine limestones were deposited in a shallow playa lake environment that ranged from lagoonal (abundance of micrite and the presence of evaporites) to offshore (presence of massive laminated micrite) (Grier, 1984).

$^{40}Ar/^{39}Ar$ geochronology of a rhyolite flow at the base of the lacustrine interval in the SPB indicates that sedimentation began after $\sim$30.7 Ma (Martinez, 1999). Deposition of $\sim$20 Ma volcanic ashes and mega-breccia sheets (Martinez et al., 1998; Martinez, 1999) at the top of the sampled section provides an upper bound for the age of lacustrine deposition in the basin (Fig. 3).

2.1. Isotopic data from the Sacramento Pass supradetachment basin

$\delta^{18}O$ values of lacustrine limestone and marl display decreasing $\delta^{18}O_{calcite}$ values from 0 to 40 m (Fig. 3 and Table 1; see Appendix A for stable isotope analytical procedures) and upsection attain low $\delta^{18}O_{calcite}$ values of $+8.3$‰ with an average of $+11.5 \pm 1.5$‰ (SMOW) within the 40–90 m depth interval. Towards the top of the section (90–120 m) $\delta^{18}O_{calcite}$ values increase by roughly 8–9‰. These changes in $\delta^{18}O_{calcite}$ values are accompanied by $(Sr/Ca)_{calcite}$ ratios that follow a similar trend with low $(Sr/Ca)_{calcite}$ in the 40–90 m interval and increasing $(Sr/Ca)_{calcite}$ towards the top of the section (Fig. 3 and Table 1).

Using paleofloral temperature estimates of 13 ± 3 °C in the nearby House Range basin (Gregory-Wodzicki, 1997), the oxygen isotope calcite–water fractionation of Kim and O'Neil (1997), and measured $\delta^{18}O_{calcite}$ collected over the 40–90 m interval, the water from which carbonates precipitated had oxygen isotopic compositions as low as $\delta^{18}O_{water} = -19.1 \pm 1.7$‰ (error calculation in Supplementary Table 1).

2.2. Isotopic data from NSRD mylonite

Muscovite δD values in mylonitic quartzite and schist collected over ca. 100 m of footwall mylonite beneath the NSRD are as low as $\delta D \leq -150$‰ with one exception at 15–25 m structural depth below the NSRD, where $\delta D_{muscovite}$ increases rapidly to high values (-76‰) (Fig. 3 and Table 2; see Appendix A for stable isotope analytical procedures). The low $\delta D_{muscovite}$ values within

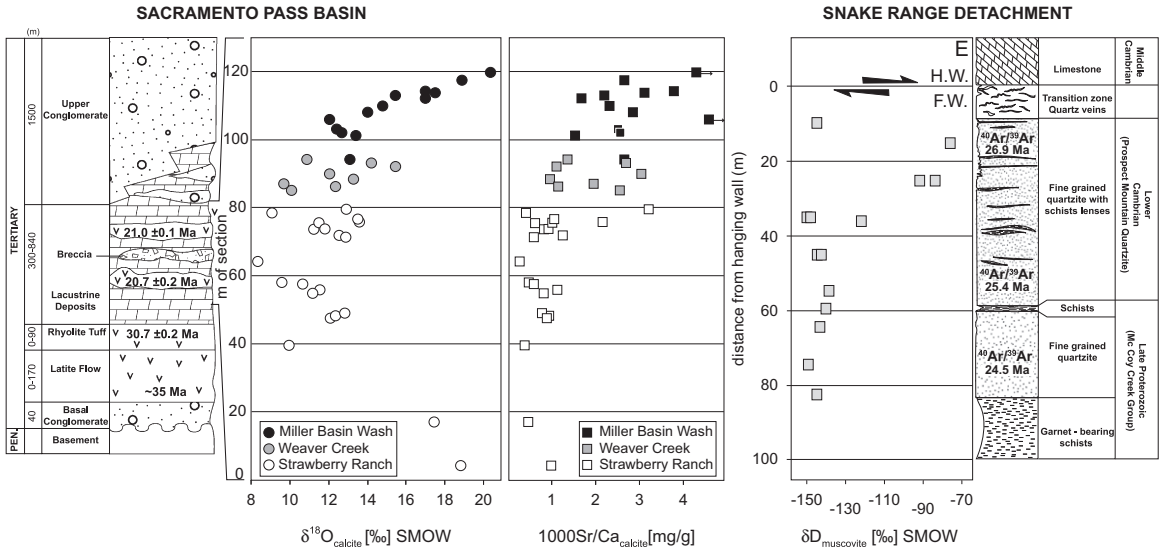

Fig. 3. Comparison of $\delta^{18}O$ values and trace-element ratios of lacustrine carbonate from the Sacramento Pass Basin and δD values of muscovite from mylonitic quartzite in the footwall of the Northern Snake Range Detachment, NV. Extremely low $\delta^{18}O$ (Sacramento Pass Basin) and δD (detachment muscovite) values characterize major parts of both proxy data sets.

Table 1
Oxygen isotope data and element ratios for lacustrine carbonates exposed in the Sacramento Pass Basin, Nevada.

Sample	Sr/Ca	δ18O (per mil) (SMOW)	Stratigraphic level (m)	Latitude	Longitude
SP-MBW-01-05	0.0052	20.4	120	N39°07′50.8″	W114°13′51.9″
SP-MBW-02-05	0.0027	18.9	117		
SP-MBW-06-05	0.0038	16.9	114		
SP-MBW-07-05	0.0031	17.5	113.5		
SP-MBW-03-05	0.0022	15.5	113	N39°07′51.3″	W114°13′49.3″
SP-MBW-08-05	0.0017	17.0	112	N39°07′49.7″	W114°13′47.0″
SP-MBW-09-05	0.0023	14.8	110	N39°07′51.1″	W114°13′43.2″
SP-MBW-10-05	0.0028	14.0	108		
SP-MBW-11-05	0.0095	12.0	106		
SP-MBW-12-05	0.0025	12.4	103		
SP-MBW-13-05	0.0015	13.4	101		
SP-MBW-14-05	0.0025	12.7	102	N39°07′51.2″	W114°13′41.0″
SP-MBW-17-05	0.0026	13.2	94	N39°07′48.4″	W114°13′40.3″
SP-WC-08-05	0.0013	10.9	94	N39°05′54.4″	W114°17′20.9″
SP-WC-07-05	0.0027	14.2	93	N39°05′54.4″	W114°17′20.9″
SP-WC-06-05	0.0011	15.5	92	N39°05′54.4″	W114°17′20.9″
SP-WC-05-05	0.0030	12.1	90	N39°05′54.4″	W114°17′20.9″
SP-WC-04-05	0.0010	13.3	88	N39°05′54.4″	W114°17′20.9″
SP-WC-03-05	0.0020	9.7	87	N39°05′54.4″	W114°17′20.9″
SP-WC-02-05	0.0011	12.4	86	N39°05′54.4″	W114°17′20.9″
SP-WC-01-05	0.0025	10.1	85	N39°05′54.4″	W114°17′20.9″
SP-SR-01-05	0.0032	12.9	80	N39°06′35.1″	W114°13′34.4″
SP-SR-02-05	0.0004	9.0	79	N39°06′35.2″	W114°13′27.9″
SP-SR-03-05	0.0010	13.5	77		
SP-SR-04-05	0.0010	13.6	76.5		
SP-SR-05-05	0.0006	11.5	76		
SP-SR-07-05	0.0008	11.8	74.5		
SP-SR-08-05	0.0009	11.2	74.2		
SP-SR-09-05	0.0012	12.6	72.5	N39°06′33.9″	W114°13′26.1″
SP-SR-10-05	0.0006	12.9	72	N39°06′33.9″	W114°13′26.1″
SP-SR-12-05	0.0003	8.3	64.5	N39°06′33.2″	W114°13′25.1″
SP-SR-13-05	0.0005	9.6	58.5		
SP-SR-14-05	0.0006	10.6	58		
SP-SR-15-05	0.0011	11.5	56.5		
SP-SR-16-05	0.0008	11.2	55	N39°06′32.2″	W114°13′19.0″
SP-SR-17-05	0.0008	12.8	50		
SP-SR-18-05	0.0010	12.4	49	N39°06′30.3″	W114°13′18.7″
SP-SR-19-05	0.0009	12.1	48		
SP-SR-20-05	0.0003	9.9	40		
SP-SR-21-05	0.0005	17.4	18	N39°06′28.5″	W114°13′15.9″
SP-SR-22-05	0.0010	18.8	5	N39°06′22.2″	W114°13′22.3″

Table 2
Hydrogen isotope composition of muscovite, footwall mylonite of the Northern Snake Range Detachment, Nevada.

Sample	δDms (per mil)	Fraction size (mm)	Distance to hanging wall (m)	Universal transverse mercator coordinates (WGS84 projection)	
SR08-3	−145	$100<f<180$	10	11S0752452	4344296
SR08-4	−76	$100<f<180$	15	11S0752389	4344323
SR08-5A	−84	$100<f<180$	25	11S0752357	4344330
SR08-5B	−92	$100<f<180$	25	11S0752357	4344330
SR08-6A	−148	$100<f<180$	35	11S0752334	4344311
SR08-6A	−150	$180<f<250$	35	11S0752334	4344311
SR08-6B	−122	$180<f<250$	35	11S0752334	4344311
SR08-7	−144	$180<f<250$	45	11S0752335	4344289
SR08-7	−144	$100<f<180$	45	11S0752335	4344289
SR08-8	−139	$100<f<180$	55	11S0752338	4344201
SR08-9	−140	$100<f<180$	60	11S0752395	4344117
SR08-10	−143	$100<f<180$	65	11S0752352	4344153
SR08-11A	−149	$180<f<250$	75	11S0752343	4344139
SR08-12	−145	$100<f<180$	83	11S0752361	4344111

the uppermost part of NSRD footwall mylonite are consistent with recrystallization of muscovite in the presence of meteoric water with δD_{water} values of $-113.0+11.5/-10.8$‰ (error calculation in Supplementary Table 1) at the inferred temperature of ductile deformation and isotopic equilibration of 402 ± 52 °C (Gébelin et al., 2011).

3. Buckskin Mountains

The northeast-dipping Buckskin Mountains Detachment (BMD) accommodated 55–75 km of early and middle Miocene extensional displacement (Richard et al., 1990; Spencer and Reynolds, 1989, 1991) and exhumed footwall rocks of the Buckskin Mountains MCC (Fig. 1). Lower plate metasedimentary rocks and Proterozoic gneisses are overprinted by a greenschist facies mylonitic fabric that developed some 7–12 Ma after the onset of extensional tectonic denudation at ca. 27 Ma (Scott et al., 1998).

3.1. Stable isotope data

We measured δD values of muscovite, chlorite, and/or epidote in 14 samples of mylonitic quartzite, microbreccia, and carbonate veins across ca. 130 m of structural section from the BMD into the underlying mylonitic footwall (Fig. 4A, Table 3; see Appendix A for stable isotope analytical procedures). $\delta D_{chlorite}$ values show small variations from −77‰ to −93‰ (SMOW). $\delta D_{muscovite}$

Table 3
Hydrogen and oxygen isotope data, footwall mylonite of the Buckskin Mountains Detachment, Arizona.

Sample	δDms (per mil)	δDchl (per mil)	δDepi (per mil)	d18Ocalcite (per mil) (SMOW)	Distance to hanging wall (m)	Universal transverse mercator coordinates (WGS84 projection)	
BU09_039		−92.7			0	12S0240311	3773532
BU09_006		−88.8			0	12S0252996	3784185
BU09_006			−62.1		0	12S0252996	3784185
BU09_37				20.4	15	12S0240379	3773565
BU09_40				22.7	15	12S0240296	3773537
BU09_036		−82.6			20	12S0240311	3773532
BU09_32				21.1	22	12S0240379	3773565
BU09_33				21.5	22	12S0240379	3773565
BU09_33				21.0	22	12S0240379	3773565
BU09_49				21.2	70	12S0236337	3772554
BU09_048		−77.3			80	12S0236337	3772554
BU09_047		−77.3			80	12S0236337	3772554
BU09_045		−89.3			100	12S0235572	3784063
BU09_044		−89.7			100	12S0235572	3784063
BU09_043		−90.8			100	12S0235572	3784063
BU09_043		−89.0			100	12S0235572	3784063
BU09_003	−67.5				100	12S0236337	3772554
BU09_002	−68.9				101	12S0236337	3772554
BU09_001	−66.0				102	12S0236337	3772554
BU09_02 A	−68.0				117	12S0236337	3772554
BU09_19				21.8	125	12S0238543	3772391
BU09_20				20.3	125	12S0238543	3772391
BU09_21				21.6	125	12S0238543	3772391
BU09_28				21.9	125	12S0238710	3771960
BU09_29				22.0	125	12S0238710	3771960

values are typically less negative ranging from −66‰ to −69‰ and one epidote sample yields a δD value of −62‰.

Previous stable isotope studies in the same area estimated temperatures of detachment faulting between 350 and 430 °C (Morrison and Anderson, 1998). Using the average δD_{ms} values within the BMD footwall and a temperature of 390 ± 40 °C, water that infiltrated the detachment had equilibrium δD_{water} values of −36 ± 6 (using hydrogen isotope fractionation equation of Suzuoki and Epstein, 1976). These values are consistent with δD_{water} values of −54 ± 6‰ (Fig. 6) calculated from the δD_{chl} values at temperatures of 390 ± 40 °C using the hydrogen isotope chlorite–water fractionation equations of Graham et al. (1984). $\delta^{18}O_{calcite}$ values from syntectonic carbonate veins average 21.4 ± 0.7‰ (Fig. 4A, Table 3).

3.2. $^{40}Ar/^{39}Ar$ geochronology

We evaluate the timing of synkinematic white mica crystallization and associated water–muscovite hydrogen isotope exchange through furnace step heating $^{40}Ar/^{39}Ar$ geochronology (analytical procedures in Supplementary Table 2). A multigrain muscovite separate from mylonitic quartzite of the BMD footwall (BU09-001) provides a plateau age of 20.8 ± 0.1 Ma (99.1% of total ^{39}Ar released; Fig. 4B and Supplementary Table 3). This $^{40}Ar/^{39}Ar$ muscovite age is in agreement with mid-Tertiary ages (~15–27 Ma) of kinematically equivalent mylonite rocks that occur in the Whipple, Buckskin, and Rawhide Mountains (see Bryant and Wooden, 1989; Richard et al., 1990; Scott et al., 1998; Wright et al., 1986).

4. House Range basin

About 40 m of white-to-tan-to-pinkish lacustrine limestone represent remnants of a relatively shallow intermountain lake (Gregory-Wodzicki, 1997) situated in the House Range (UT; Fig. 1). Lacustrine limestone is micritic to vuggy, indicating primary porosity due to buried plant stems and/or degraded organic matter. A 31.4 ± 0.5 Ma ash-flow tuff ($^{40}Ar/^{39}Ar$ plagioclase; McIntosh in Gregory-Wodzicki, 1997) marks the top of the section (Fig. 5).

4.1. Stable isotope data

In contrast to the SPB, $\delta^{18}O_{calcite}$ values in the House Range basin occupy a narrow range and average 18.4 ± 0.8‰ (Fig. 5, Table 4; see Appendix A for stable isotope analytical procedures). We are unable to evaluate the degree of evaporative ^{18}O enrichment in the paleolake but the restricted $\delta^{18}O_{calcite}$ values suggest uniform lake water compositions throughout the history of carbonate deposition. Using a mean annual temperature of 13 ± 3 °C (Gregory-Wodzicki, 1997) and fractionation equations of Kim and O'Neil (1997) average $\delta^{18}O_{water}$ values were −12.2 ± 1.1‰ (error calculation in Supplementary Table 1).

5. Discussion

5.1. Sacramento Pass Basin oxygen isotope record

The SPB $\delta^{18}O_{calcite}$ data display a large range from +8.3‰ to +20.4‰ (SMOW; see Fig. 3 and Table 1) with exceptionally low $\delta^{18}O_{calcite}$ (+8.3‰ to +13.6‰) that characterize most of the measured stratigraphic section. Relatively high $\delta^{18}O_{calcite}$ values at the base and top of the section (0–20 m and >90 m) contrast the low $\delta^{18}O_{calcite}$ values (40–90 m) that are paralleled by lower Sr/Ca (0.0003–0.003; Fig. 3 and Table 1). These low $(Sr/Ca)_{calcite}$ values are indicative of open system lake behavior, with lower paleosalinity (Chivas et al., 1993) and continuous freshwater input to the lake. In contrast, we interpret the high $\delta^{18}O_{calcite}$ values at the top and bottom of the section to reflect increasingly evaporative lake conditions. During evaporation, oxygen isotope fractionation induces an enrichment of ^{18}O (and D) in surface water from which lacustrine carbonates precipitate (e.g. Fontes

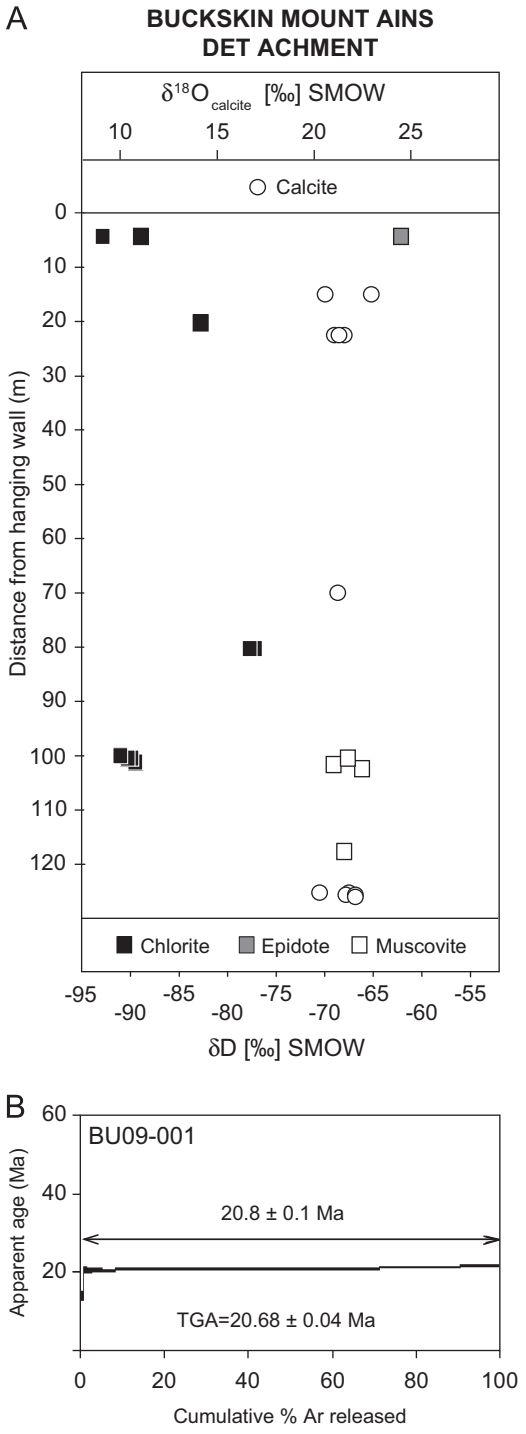

Fig. 4. (A) δD values of muscovite, chlorite, and epidote from mylonitic quartzite and microbreccia and $\delta^{18}O_{calcite}$ from carbonate veins in the footwall of the Buckskin Mountains Detachment, AZ. (B) $^{40}Ar/^{39}Ar$ step-heating spectrum of muscovite fish from the Buckskin Mountains Detachment footwall (sample BU09-001).

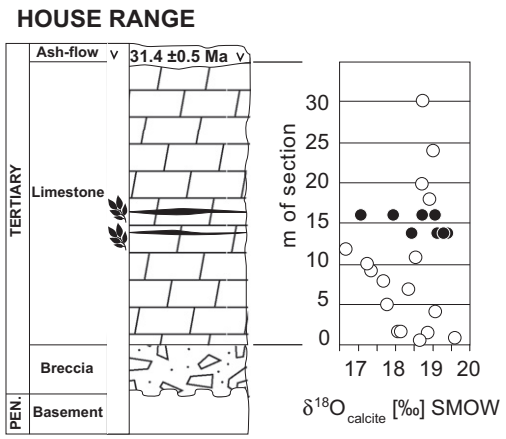

Fig. 5. $\delta^{18}O$ values of lacustrine carbonate from the House Range basin. Black circles indicate $\delta^{18}O$ values obtained from lake beds that provided flora for leaf-physiognomy based paleoaltimetry estimates (Gregory-Wodzicki, 1997).

Table 4
Oxygen isotope data for lacustrine limestones collected in the House Range, Utah.

Sample	d18O	Stratigraphic level (m)	Universal Transverse Mercator Coordinates (WGS84 Projection)	
06HR001	18.6	0	12S0304682	4350109
06HR002	19.6	1	12S0304682	4350109
06HR003	18.9	1.50	12S0304682	4350109
06HR004	18.1	1.6	12S0304682	4350109
06HR005	18.1	1.7	12S0304682	4350109
06HR006	19.1	4	12S0304682	4350109
06HR007	17.8	5	12S0304682	4350109
06HR008	18.3	7	12S0304682	4350109
06HR009	17.7	8	12S0304682	4350109
06HR010	17.3	9	12S0304682	4350109
06HR011	17.2	10	12S0304682	4350109
06HR012	18.5	11	12S0304682	4350109
06HR013	16.7	12	12S0304682	4350109
06HR014	18.4	14	12S0304682	4350109
06HR015	17.9	16	12S0304682	4350109
06HR016	18.9	18	12S0304682	4350109
06HR018	18.7	20	12S0304682	4350109
06HR020	19.0	24	12S0304682	4350109
06HR022	18.7	30	12S0304682	4350109
06HR024A	19.2	14	12S304672	4350173
06HR024D	19.2	14	12S304672	4350173
06HR024H	19.1	14	12S304672	4350173
06HR023A	17.1	16	12S0304685	4350234
06HR023E	19.0	16	12S0304685	4350234
06HR023J	18.7	16	12S0304685	4350234

and Gonfiantini, 1967; Gat, 1981). Evaporative SPB lake conditions during precipitation of high-$\delta^{18}O$ calcite are supported by both increased $(Sr/Ca)_{calcite}$ values indicative of elevated paleosalinity and by the presence of dolomite, gypsum, and anhydrite.

Evaporation controls the rate of change of $\delta^{18}O$ in a lake and is dependent upon lake surface area and volume (e.g. Benson et al., 1996). The decrease in $\delta^{18}O_{calcite}$ values in the SPB record is therefore consistent with an increase in freshwater input and a resulting increase in lake volume. Such vertical variations are recorded through time within the depositional environment showing signs of periodic emergence (equant and irregular fenestral fabrics, mud cracks, anhydrite replaced by chalcedony, and calcite pseudomorphing gypsum within the lagoonal facies) in the shallow playa lake, its size (perimeter ca. 18 km) being three times smaller than the present area of exposure (Grier, 1984). Therefore, the high $\delta^{18}O_{calcite}$ values illustrate one or more episodes of low lake levels during which evaporation outpaced fresh water input to the lake.

We consider the 11.5 ± 1.5‰ average of the low-$\delta^{18}O$ calcite to be representative of lacustrine $\delta^{18}O$ values being least affected by evaporation and therefore most appropriate to calculate meteoric $\delta^{18}O_{water}$ values. These attain -19.1 ± 1.7‰ based on 13 ± 3 °C oxygen isotope exchange temperatures (Gregory-Wodzicki, 1997) and calcite–water equilibrium fractionation (Kim and O'Neil, 1997).

5.2. Northern Snake Range coupled basin-detachment systems

The low $\delta^{18}O$ values of meteoric water calculated from the SPB limestone are in good agreement with syntectonic meteoric fluid compositions found in the NSRD. At Hendry's Creek (Fig. 2), muscovite-bearing quartzite in the mylonitic footwall recrystallized in the presence of meteoric water with δD_{water} of $-113+12/-11‰$ (Gébelin et al., 2011 and Supplementary Table 1). These low δD_{water} values reflect a time-integrated average of catchment-wide precipitation and near-surface groundwater sourced at higher elevations that penetrated the actively extending crust down to the brittle–ductile transition (e.g. Fricke et al., 1992; Mulch et al., 2004, 2007). At such depths, neocrystallized synkinematic white mica equilibrated with evolved meteoric water over the time scale of the mylonitic deformation that lasted from 27 Ma to at least 23 Ma (Gébelin et al., 2011).

These stable isotope data together with the lacustrine carbonate record extend previously established meteoric water compositions ($\delta^{18}O_{water} \leq -12‰$ and $\delta D_{water} \leq -86‰$ at $T=120$–$300\ ^{\circ}C$; Losh, 1997) based on $\delta D_{silicate}$ values in granodiorite and mylonite of the NSRD footwall of $-145‰$ to $-125‰$, $\delta^{18}O$ values of stylolitic calcite breccia in the NSRD hanging wall ranging from $-1.6‰$ to $+15.3‰$, and calcite from NSRD hanging wall faults that cover $\delta^{18}O$ values between $-2.4‰$ and $+16.3‰$ (Losh, 1997) to even lower values. The extremely low δD_{water} and $\delta^{18}O_{water}$ values obtained at various crustal levels (syndetachment basin, fractured hanging wall, mylonitic footwall) and different proxy materials (lacustrine carbonate, vein calcite, stylolite, white mica) therefore provide a robust record of paleo-meteoric water composition and are consistent with meteoric water sourced from high elevation catchment regions in the Snake Range MCC during exhumation and rock uplift.

5.3. Air mass trajectories and paleogeography of the North American Cordillera

Topography exerts an important control on atmospheric moisture fluxes over western North America, and conversely the topographic history of the region may have directly influenced long-term patterns of regional temperature and rainfall (e.g. Galewsky, 2009). Today, the climate of the western United States is influenced by the direct competition of two air masses that originate from the Pacific Ocean and from the Gulfs of Mexico and California (Bryson and Hare, 1974; Liu et al., 2010). Five distinct regions contribute to precipitation in the Great Basin: (1) Gulf of Alaska and north Pacific, (2) central Pacific, (3) tropical Pacific, (4) Gulf of Mexico and (5) the continental interior of the western U.S. (Friedman et al., 2002a). For stations located in North Central Nevada (Winnemucca) more than half of the total precipitation originates from the tropical Pacific whereas air mass trajectories causing precipitation at Cedar City (Utah) located about 180 km from the SPB have their main source of precipitation in the north, central, and tropical Pacific with only 9% recycled moisture, and 4% originating from the Gulf of Mexico (Friedman et al., 2002a).

Calculated Miocene Snake Range δD_{water} ($-113+12/-11‰$) and $\delta^{18}O_{water}$ ($-19.1\pm1.7‰$) values are similar to modern hydrogen (and oxygen) isotopes in precipitation over Nevada ($-115‰$ at Mt. Moriah, Friedman et al., 2002b; see also Fig. 6). However, Miocene paleogeographic reconstructions of western North America (Fig. 1B) show that: (1) the distance separating the Snake Range from the Pacific Ocean was less than what it is today ($\sim$200 km difference along an E–W transect across the northwestern U.S.); (2) no Transverse Ranges separated the Great Basin from the Pacific Ocean (Blythe et al., 2000); and (3) the Gulf of California did not exist.

Evaluating the impact of climate (and topography) change on western North American air mass trajectories (e.g. Galewsky, 2009) is beyond the scope of this study. However, to first-order past differences in paleogeography, upstream topography, and paleoclimate should translate into more positive Oligo-Miocene $\delta^{18}O$ and δD values of precipitation in the Snake Range MCC because: (1) increased distance from the water vapor source yields a systematic pattern of decreasing $\delta^{18}O$ (and δD) values of precipitation (ca. $-1.6‰$ to $-3.2‰$/100 km for δD; Dansgaard, 1964; Rozanski et al., 1993); (2) the modern Transverse Ranges of California induce a depletion in ^{18}O and D in precipitation on the leeward side (the "isotopic rain shadow", Siegenthaler and Oeschger, 1980); and (3) isotopic lapse rates are reduced in a warmer Miocene paleoclimate due to enhanced upper troposphere warming (Poulsen and Jeffery, 2011). Generally higher δD and $\delta^{18}O$ values in precipitation during a warmer Miocene climate are consistent with relatively high Miocene $\delta D_{precipitation}$ values at the near-coastal site (Buckskin Mountains) that are unlikely to be affected by major elevation change since the Miocene.

5.4. Oligo-Miocene paleotopography of eastern Nevada

How high was the Snake Range region during the Oligo-Miocene? For our paleoelevation reconstruction we compare Miocene $\delta^{18}O_{water}$ and δD_{water} values obtained from the NSRD mylonitic footwall and

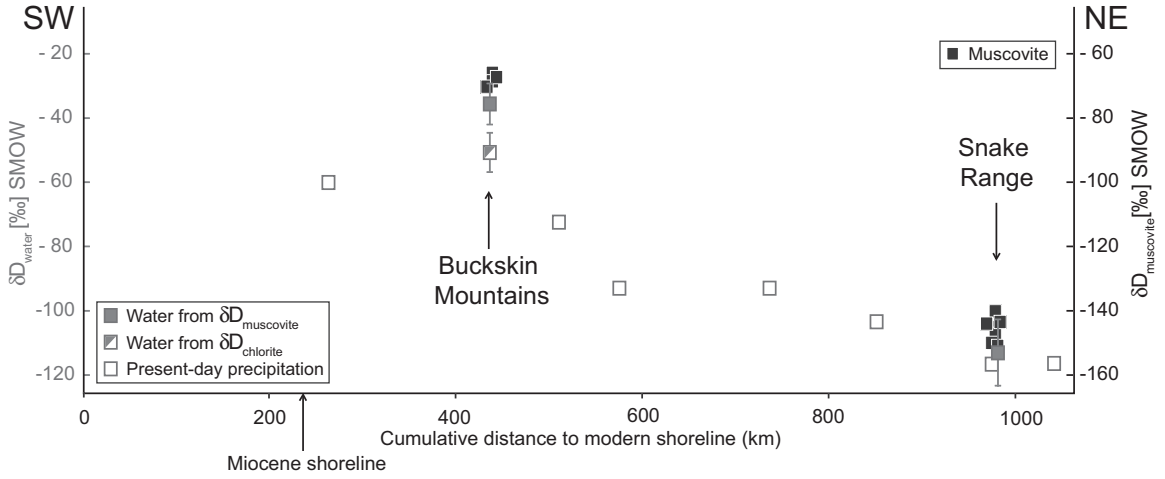

Fig. 6. δD of meteoric fluids in age-equivalent fault environments. A 77‰ difference in δD_{water} calculated from the $\delta D_{muscovite}$ of the Snake Range and the Buckskin Mountains indicates an elevation difference between the two areas of about 3850 ± 650 m in elevation.

SPB lacustrine carbonate with those acquired from the Buckskin Mountains, which at the time were located near sea level and obtained moisture from similar sources as the Snake Range region. Such an approach relating high-elevation stable isotope records to climate-controlled near-sea level records eliminates some of the assumptions commonly made in stable isotope paleoaltimetry (e.g. Mulch and Chamberlain, 2007) and reduces uncertainties due to lack of knowledge of paleoclimate variations on isotope in precipitation patterns.

(1) Paleogeographic reconstructions (Fig. 1B) place the Miocene Buckskin Mountains close to the Pacific Coast and deformation of marine-estuarine deposits in the Bouse basin (eastern Vidal Valley, SE California) in response to extension along the Whipple–Buckskin–Harquahala detachment supports the idea that the BMD was active just before the transgression that formed the Gulf of California (Buising, 1988, 1990). Our relatively high δD_{water} values (-36 ± 6‰) calculated from muscovite in the BMD are consistent with a near-coastal position and indicate meteoric water sourced at low elevations. Even though only broadly similar in their relative deformation chronologies and detachment dynamics, our stable isotope data suggest that Oligo-Miocene (27–20 Ma) meteoric fluid compositions within the Snake Range ($\delta D_{water}\sim-113$‰) and Buckskin Mountains ($\delta D_{water}\sim-36$‰) detachments and mylonitic footwall were vastly different ($\Delta\delta D_{water}=-77$‰, Fig. 6 and Supplementary Table 1). Since the stable isotopic composition of water scales with elevation ("altitude effect" of ca. -2.8‰ in $\delta^{18}O$ or ca. -20‰ in δD per km; e.g. Poage and Chamberlain, 2001; Rowley and Currie, 2006; Rowley and Garzione, 2007; Quade et al., 2011), the difference in the isotopic composition of Miocene meteoric water between the Snake Range and the Buckskin Mountains is consistent with an elevation difference on the order of 3850 ± 650 m (Fig. 6 and Supplementary Table 1). Additional paleoelevation information in the central Great Basin comes from a comparison between $\delta^{18}O_{water}$ from the Sacramento Pass Basin (-19.1 ± 1.7‰) and the BMD (-5.8 ± 0.8‰), that translates into an elevation difference of 4785 ± 680 m (Supplementary Table 1).

We complement our Snake Range paleoelevation estimate by further comparing our ~20 Ma Buckskin Mountains MCC $\delta D_{muscovite}$ data with the $\delta^{18}O_{calcite}$ record from the late Eocene ~35 Ma House Range (UT, USA, Fig. 2) for which leaf physiognomy provides paleoelevation estimates of 2.9 ± 1.5 km to 3.6 ± 0.7 km (Gregory-Wodzicki, 1997). Given the relatively large age difference between the two records such an attempt can only serve as a first approximation, and Oligo-Miocene paleoelevation reconstructions in the central Great Basin need further refinement. Assuming that first-order air mass trajectories (and sources) did not change significantly over the time interval of interest for the Great Basin region (see above), the -6.5‰ difference between $\delta^{18}O_{water}$ in the BMD (-5.8 ± 0.8‰) and House Range (-12.2 ± 1.1‰; Fig. 5, Table 4) is consistent with the House Range attaining elevations $\sim2300\pm500$ m higher than the Buckskin Mountains (Supplementary Table 1). This is a lower bound on potential paleoelevation estimates because sedimentological evidence (cryptalgal laminations, vuggy carbonate, oncolites) in the House Range basin indicates at least periodic evaporative enrichment in lake water ^{18}O that would lead us to underestimate the actual paleoelevation. Our minimum estimate, however, is in good agreement with paleofloral elevation estimates of 2.9 ± 1.5 km (Gregory-Wodzicki, 1997), which strengthens the idea that this part of the western North American Cordillera stood at moderate to high elevation during the Oligocene.

5.5. Cordilleran-scale significance of stable isotope paleoaltimetry data

Much of the Cenozoic evolution of the North American Cordillera is dominated by extensional tectonics and the demise of a broad orogen whose origins date back to crustal shortening and Mesozoic contraction (DeCelles, 2004). Extension occurred diachronously from north to south and coincided with surface uplift (Mix et al., 2011; Chamberlain et al., in press), magmatism (Armstrong and Ward, 1991), and formation of MCCs (Teyssier et al., 2005; Mulch et al., 2006; Foster et al., 2007). Extension and exhumation of partially molten crust occurred between 55 and 45 Ma in British Columbia (Parrish et al., 1988; Vanderhaeghe et al., 2003) and migrated to the south reaching northeastern Nevada no later than 39–35 Ma (MacCready et al., 1997) and east-central Nevada during the Oligo-Miocene (Gans et al., 1989; Miller et al., 1999a; Gébelin et al., 2011). Farther south, Basin-and-Range-type MCC evolved later, during the Middle Miocene (Howard and John, 1987; Axen et al., 1993; Scott et al., 1998).

Different models explain this N–S diachronous record either through changes in forces at the base of the lithosphere (slab roll-back from East to West, Bird, 1988; north-to-south slab peel-off, Humphreys, 1995), changes in crustal rheology and associated ductile flow (Teyssier et al., 2005) or changes in buoyancy forces within the lithosphere (Molnar and Chen, 1983; Sonder et al., 1987; Jones et al., 1996). Models suggesting lower crustal flow are in good agreement with exhumation histories of migmatite-cored MCC and imply that upper crustal extension is accommodated by lateral influx of weak lower crustal material (Block and Royden, 1990; Wernicke, 1990). According to such tectonic models, no elevation change is required locally due to isostatically compensated changes within the underlying lithosphere. Because the entire region is extending, however, collapse of the previously thickened continental crust is likely to result in lowering of regional mean elevation and associated increase in relief due to the development of fault-bounded ranges and the erosional removal of sediment (Teyssier et al., 2005).

A vast body of stable isotope paleoaltimetry data for western North America is seemingly at odds with such models as stable isotope data for early Cenozoic (65–50 Ma) rocks do not show evidence for arid, high elevation continental interiors (e.g. Mix et al., 2011; Chamberlain et al., in press). Rather, interactions of topography and atmospheric circulation and rainfall patterns characteristic of high elevation regions start to dominate western North America synchronous with the timing of core complex formation and magmatism at individual latitudes.

Here, three lines of evidence lead us to conclude that east-central Nevada was at higher-than-present elevation during the Oligo-Miocene (e.g. Wolfe et al., 1997). First, the different proxy records from the Northern Snake Range indicate low δD_{water} (and $\delta^{18}O_{water}$) values in different compartments of the meteoric hydrological system. The isotopic values are similar to modern records from the Bolivian Altiplano or Tibet and lend support to a model in which the 27–20 Ma Cordilleran hinterland sat at high elevations. Second, when applying a conservative estimate of the relationship between elevation and hydrogen isotopes in precipitation for western North America (20‰/km; e.g. Poage and Chamberlain, 2001), a ~77‰ difference in δD_{water} between the Snake Range ($\delta D_{water}\sim-113$‰) and the Buckskin Mountains ($\delta D_{water}\sim-36$‰) indicates that the two regions were separated by about 3850 ± 650 m in mean elevation (Fig. 6 and Supplementary Table 1). We are well aware of the fact that modern isotope-elevation relationships within the Basin-and-Range can vary dramatically; however, to first order, comparisons between the near Pacific and the continental interior provide a relatively robust measure of elevation for most parts of the western United States. Indeed, at such large geographic scale (>500 km), the continental effect estimated at ca. -1.6 to -3.2‰/100 km for δD (Dansgaard, 1964; Rozanski et al., 1993) becomes negligible compared to the altitude effect. Third, given the proximity to the Snake Range region, the House Range $\delta^{18}O_{calcite}$ data provide a minimum mean paleoelevation estimate of 2300 ± 500 m based on the

difference in $\delta^{18}O_{water}$ between the Buckskin Mountains MCC and the late Eocene House Range basin.

It is difficult to evaluate from the SPB and NSRD data whether the Snake Range elevation estimates are representative on a larger regional scale or depict the emergence of a tectonically active area during exhumation and rock uplift. What becomes evident from the geological record is that the relief structure in the area changed dramatically from the Oligocene into the early Miocene. The presence of large hanging wall landslide blocks intercalated with the SPB sediments points to considerable relief and steep scarps in the source region (Grier, 1984; Miller et al., 1995; Miller et al., 1999b) sometime between 23 and 20 Ma (Martinez, 1999). At that time the SPB acted as an east-west elongate, fault-bounded basin with sediment sourced to the south and southwest (Grier, 1984). Based on coarse fanglomerate, abundant gravity flows, and slideblocks, as well as braided stream deposits, the ancient basin margin was probably close to the modern margin of the basin (Grier, 1984).

Analysis of volcanic flow directions shows that a north–south topographic divide characterized central Nevada during the Eo-Oligocene (Henry, 2008). West of this divide, relief was low, which allowed Oligocene ignimbrite flows to travel over 200 km from their source in central Nevada to the western foothills of the present day Sierra Nevada (Henry, 2008; Best et al., 2009). In contrast, east of this divide structural and sedimentological studies indicate development of high relief in east-central Nevada with tall fault-bounded peaks (Druschke et al., 2009). The stable isotope paleoaltimetry reconstructions presented here integrate well with a model of increased relief structure in east-central Nevada during the Oligo-Miocene and also fit into a Cordilleran-scale context where Eocene–Oligocene highlands developed as a topographic wave swept southward along strike of the Cordilleran orogen (Mix et al., 2011; Chamberlain et al., in press). In such a model, the Snake Range represents one of the youngest high elevation terrains forming the southern tip of a continental high that started to develop in British Columbia at about 50 Ma.

6. Conclusion

Comparison of Oligo-Miocene stable isotope multi-proxy records from sites near Miocene sea level (Buckskin Mountains, AZ) and the continental interior of the Great Basin (Snake Range, NV and House Range, UT) permit paleoelevation reconstructions for the east-central part of the Great Basin. Each of the investigated compartments of the paleohydrologic system (footwall mylonite, lacustrine sediments, brittle faults) within the Snake Range MCC depicts a coherent scenario of low Oligo-Miocene meteoric $\delta^{18}O$ and δD values that, when compared to near-sea level records, are consistent with this part of the North American Cordillera being at minimum elevations of about 3850 ± 650 m between 27 and 20 Ma. Additional support for such paleoelevations comes from comparison between the Buckskin Mountains MCC and the intermountain House Range basin. Differences in $\delta^{18}O_{water}$ compositions are consistent with minimum paleoelevation for the House Range of 2300 ± 500 m, which is in good agreement with paleobotanical altimetry estimates of 2.9 ± 1.5 km (Gregory-Wodzicki, 1997). The low $\delta^{18}O$ values of meteoric water obtained from both carbonates and hydrous minerals in the Snake Range reflect precipitation captured at high elevation and suggest that high peaks surrounded the region during the early- to mid-Miocene.

Acknowledgments

This study was partially funded through a Leibniz University young investigator grant "Wege in die Forschung" to AG and through the LOEWE funding program of Hesse's Ministry of Higher Education, Research, and the Arts. AM acknowledges support through DFG-INST 187/400-1 FUGG. CPC and AM acknowledge support through NSF EAR 1019648, and CT through NSF EAR 0838541. We thank C. Wenske (Hannover) for analytical support. Editorial comments and suggestions by two anonymous journal reviewers are gratefully acknowledged.

Appendix A. Stable isotope analyses

Carbonate oxygen and hydrogen isotope measurements were performed in the Stable Isotope Laboratory at the Institut für Geologie, Leibniz Universität Hannover. Between 0.150 and 0.300 mg of carbonate powder were extracted using a dentist's drill and reacted at 72 °C with phosphoric acid (99%) in sealed reaction vessels flushed with helium gas. Headspace sampling of evolved CO_2 was performed with a Finnigan Gas-Bench II, and isotopic ratios were measured in continuous flow mode on a Delta V Advantage mass spectrometer. One internationally referenced standard material (NBS-19) and additional in-house working standards were run with the samples. Precision of the carbonate stable isotope data is ± 0.1‰ for both oxygen and carbon isotope ratios based on replicate analysis of carbonate standards.

The δD values of muscovite, chlorite, and epidote were determined by continuous flow mass spectrometry using a high temperature elemental analyzer (Thermo Finnigan TC/EA) coupled to a Delta V Advantage mass spectrometer in continuous flow mode. Three internationally referenced standard materials and additional in-house working standards were run with the samples. After correction for mass bias, daily drift of the thermal combustion reactor, and offset from the certified reference values, NBS30 (biotite), NBS22 (oil), CH7 (polyethylene foil) had $\delta D = -65.8$‰, -118.6‰, and -102.1‰, respectively. Repeated measurements of various standards and unknowns gave a precision of ± 2‰ for δD. All isotopic ratios are reported relative to standard mean ocean water (SMOW).

Appendix B. Supporting information

Supplementary data associated with this article can be found in the online version at http://dx.doi.org/10.1016/j.epsl.2012.04.029.

References

Armstrong, R.L., Ward, P., 1991. Evolving geographic patterns of Cenozoic magmatism in the North American Cordillera: the temporal and spatial association of magmatism and metamorphic core complexes. J. Geophys. Res. 96 (13), 201–213. 224.

Axen, G.J., Taylor, W.J., Bartley, J.M., 1993. Space-time patterns and tectonic controls of Tertiary extension and magmatism in the Great Basin of the western United States. Geol. Soc. Am. Bull. 105, 56–76.

Best, M.G., Barr, D.L., Christiansen, E.H., Gromme, S., Deino, A.L., Tingey, D.G., 2009. The Great Basin Altiplano during the middle Cenozoic ignimbrite flareup: insights from volcanic rocks. Int. Geol. Rev. 51, 589–633.

Benson, L., Lloyd, D.W., Rye, R., 1996. Carbonate deposition, Pyramid Lake Subbasin, Nevada: 4. Comparison of the stable isotope values of carbonate deposits (tufas) and the Lahontan lake-level record. Palaeogeogr. Palaeoclim. 122, 45–76.

Bird, P., 1988. Formation of the Rocky Mountains, western United States: a continuum computer model. Science 239, 1501–1507.

Blakey, R.C., 2011. Paleogeography of the Southwestern US. Northern Arizona University Web resource: 〈http://www2.nau.edu/rcb7/nam.html〉.

Blythe, A.E., Burbank, D.W., Farley, K.A., Fielding, E.J., 2000. Structural and topographic evolution of the central Transverse Ranges, California, from apatite fission-track, (U-Th)/He and digital elevation model analyses. Basin Res. 12, 97–114.

Block, L., Royden, L.H., 1990. Core complex geometries and regional scale flow in the lower crust. Tectonics 9, 557–567.

Bryant, B., Wooden, J.L., 1989. Lower-plate rocks of the Buckskin Mountains, Arizona: a progress report. In: Spencer,, J.E., Reynolds,, S.J. (Eds.), Geology and Mineral Resources of the Buckskin and Rawhide Mountains, west-central Arizona. Arizona Geol. Survey Bulletin 198, pp. 47–50.

Bryson, R.A., Hare, R.K., 1974. The climate of North America. In: Bryson, R.A., Hare, R.K. (Eds.), Climates of North America: World Survey of Climatology, 11. Elsevier, New York, pp. 1–47.

Buising, A.V., 1988. Depositional and tectonic evolution of the northern proto-Gulf of California and lower Colorado River, as documented in the Mio-Pliocene Bouse Formation and bracketing units, southeastern California and western Arizona. Ph.D. Dissertation. Univ. of California, Santa Barbara, 196 pp..

Buising, A.V., 1990. The Bouse formation and bracketing units, southeastern California and Western Arizona: implications for the evolution of the proto-Gulf of California and the lower Colorado River. J. Geophys. Res. 95, 20111–20132.

Chamberlain, C.P., Poage, M., Craw, D., Reynolds, R., 1999. Topographic development of the Southern Alps recorded by the isotopic composition of authigenic clay minerals, South Island, New Zealand. Chem. Geol. 155, 279–294.

Chamberlain, C.P., Mix, H.T., Mulch, A., Hren, M.T., Kent-Corson, M.L., Davis, S.J., Horton, T., Graham, S.A.. The Cenozoic climatic and topographic evolution of the Western North American Cordillera. Am. J. Sci., in press.

Chivas, A.R., De Deckker, P., Cali, J., Chapman, A., Kiss, E., Shelley, J., 1993. Coupled stable isotope and trace element measurements of lacustrine carbonates as paleoclimatic indicators. In: Swart, P., Lohamnn, K., Mckenzie, J., Savin, S. (Eds.). Climate change in continental isotopic records. Geophys. Monogr. 78, pp. 113–122.

Dansgaard, W., 1964. Stable isotopes in precipitation. Tellus 16, 436–468.

Davis, S.J., Mulch, A., Carroll, A.R., Horton, T.W., Chamberlain, C.P., 2009. Paleogene landscape evolution of the central North American Cordillera: developing topography and hydrology in the Laramide foreland. Geol. Soc. Am. Bull. 121, 100–116, http://dx.doi.org/10.1130/B26308.1.

DeCelles, P.G., 2004. Late Jurassic to Eocene evolution of the Cordilleran thrust belt and foreland basin systems, western USA. Am. J. Sci. 304, 105–168.

DeCelles, P.G., Lawton, T.F., Mitra, G., 1995. Thrust timing, growth of structural culminations, and synorogenic sedimentation in the type Sevier orogenic belt, western USA. Geology 23, 699–702.

Druschke, P., Hanson, A.D., Wells, M.L., 2009. Structural, stratigraphic, and geochronologic evidence for extension predating Palaeogene volcanism in the Sevier hinterland, east-central Nevada. Int. Geol. Rev. 51, 743–775.

Folk, R.L., 1974. The natural history of crystalline calcium carbonate; effect of magnesium content and salinity. J. Sediment. Petrol. 44, 40–53.

Fontes, J.C., Gonfiantini, R., 1967. Fractionnement isotopique de l'hydrogène dans l'eau de crystallization du gypse. C. R. Acad. Sci. Paris 265, 4–6.

Foster, D., Doughty, P.T., Kalakay, T.J., Fanning, C.M., Coyner, S., Grice, W.C., Vogl, J., 2007. Kinematics and timing of exhumation of metamorphic core complexes along the Lewis and Clark Fault Zone. Geol. Soc. Am. Spec. Paper 434, 207–232.

Fricke, H.C., Wickham, S.M., O'Neil, J.R., 1992. Oxygen and hydrogen isotope evidence for meteoric water infiltration during mylonitization and uplift in the Ruby Mountains-East Humboldt Range core complex, Nevada. Contrib. Mineral. Petrol. 111, 203–221.

Friedman, I., Harris, J.M., Smith, G.I., Johnson, C.A., 2002a. Stable isotope composition of water in the Great Basin, United States 1: Air-mass trajectories. J. Geophys. Res. 107, 14,1–14,14.

Friedman, I., Smith, G.I., Johnson, C.A., Moscati, R.J., 2002b. Stable isotope composition of water in the Great Basin, United States 2: modern precipitation. J. Geophys. Res. 107, 15,1–15,22.

Galewsky, J., 2009. Orographic precipitation isotope ratios in stratified atmospheric flows: implications for paleoelevation studies. Geology 37, 791–794, h ttp://dx.doi.org/10.1130/G30008A.1.

Gans, P.B., Mahood, G.A., Schermer, E., 1989. Synextensional magmatism in the Basin and Range Province: a case study from the eastern Great Basin. Geol. Soc. Am. Spec. Pap.. vol. 223, pp. 53.

Garzione, C.N., Molnar, P., Libarkin, J.C., MacFadden, B.J., 2006. Rapid late Miocene rise of the Bolivian Altiplano: evidence for removal of mantle lithosphere. Earth Planet. Sci. Lett. 241, 543–556.

Garzione, C.N., Quade, J., DeCelles, P.G., English, N.B., 2000. Predicting paleoelevation of Tibet and the Himalaya from δ18O vs. altitude gradients in meteoric water across the Nepal Himalaya. Earth Planet. Sci. Lett. 183, 215–229.

Gat, J.R., 1981. Lakes. In: Gat, J.R., Gonfiantini, R. (Eds.). Stable Isotope Hydrology: Deuterium and Oxygen-18 in the Water Cycle. Int. At. Energy Agency. Tech. Rep. vol. 210, pp. 203–221.

Gébelin, A., Mulch, A., Teyssier, C., Heizler, M., Vennemann, T., Seaton, N.C.A., 2011. Oligo-Miocene extensional tectonics and fluid flow across the Northern Snake Range detachment system, Nevada. Tectonics 30 (1–18), TC5010, http://dx.doi.org/10.1029/2010TC002797.

Graham, C.M., Atkinson, J., Harmon, R.S., 1984. Hydrogen isotope fractionation in the system chlorite-water. N. E. R. C. In: 6th Progress Report of Research 1981–1984, N. E. R. C. Publication Series D 25, p. 139.

Gregory-Wodzicki, K.M., 1997. The Late Eocene House Range flora, Sevier desert, Utah: paleoclimate and paleoelevation. Palaios 12, 552–567.

Grier, S.P., 1984. Alluvial fan and lacustrine carbonate deposits in the Snake Range: a study of Tertiary sedimentation and associated tectonism. M.S. Thesis, Stanford University, Standford, CA, 61 pp.

Henry, C.D., 2008. Ash-flow tuffs and paleovalleys in northeastern Nevada: implications for Eocene paleogeography and extension in the Sevier hinterland, northern Great Basin. Geosphere 4, 1–35.

Horton, T.W., Chamberlain, C.P., 2006. Stable isotopic evidence for Neogene surface downdrop in the central Basin and Range province. Geol. Soc. Am. Bull. 118, 475–490.

Horton, T.W., Sjostrom, D.J., Abruzzese, M.J., Poage, M.A., Walbauer, J.R., Hren, M., Wooden, J., Chamberlain, C.P., 2004. Spatial and temporal variation of Cenozoic surface elevation in the Great Basin and Sierra Nevada. Am. J. Sci. 304, 862–888.

Howard, K.A., John, B.E., 1987. Crustal extension along a rooted system of imbricate low-angle faults: Colorado River extensional corridor, California and Arizona. In: Coward, M.P., Dewey, J.F., Hancock, P.L. (Eds.), Continental Extensional Tectonics, vol. 28. Geol. Soc. Spec. Publ. London, pp. 299–311.

Hren, M.T., Pagani, M., Erwin, D.M., Brandon, M., 2010. Biomarker reconstruction of the early Eocene paleotopography and paleoclimate of the northern Sierra Nevada. Geology 38, 7–10.

Humphreys, E.D., 1995. Post-Laramide removal of the Farallon slab, western United States. Geology 23, 987–990.

Jones, C.H., Unruh, J.R., Sonder, L.J., 1996. The role of gravitational potential energy in active deformation in southwestern United States. Nature 381, 37–41.

Kent-Corson, M.L., Sherman, L.S., Mulch, A., Chamberlain, C.P., 2006. Cenozoic topographic and climatic response to changing tectonic boundary conditions in Western North America. Earth Planet. Sci. Lett. 252, 453–466.

Kim, S.T., O'Neil, J.R., 1997. Equilibrium and non-equilibrium oxygen isotope effects in synthetic carbonates. Geochim. Cosmochim. Acta 61, 3461–3475.

Liu, Z., Bowen, G.J., Welker, J.M., 2010. Atmospheric circulation is reflected in precipitation isotope gradients over the conterminous United States. J. Geophys. Res. 115, D22120, http://dx.doi.org/10.1029/2010JD014175.

Lee, J., Miller, E.L., Sutter, J.F., 1987. Ductile strain and metamorphism in an extensional tectonic setting: a case study from the northern Snake Range, Nevada, USA. In: Coward, M.P., Dewey, J.F., Hancock, P.L. (Eds.), Continental Extensional Tectonics. Geol. Soc. Spec. Publ., London, pp. 267–298.

Losh, S., 1997. Stable isotope and modeling studies of fluid-rock interaction associated with the Snake Range and Mormon Peak detachment faults, Nevada. Geol. Soc. Am. Bull. 109, 300–323.

MacCready, T., Snoke, A.W., Wright, J.E., Howard, K.A., 1997. Mid-crustal flow during Tertiary extension in the Ruby Mountains core complex, Nevada. Geol. Soc. Am. Bull. 109, 1576–1594.

Martinez, C.M., 1999. Tertiary sedimentation in the Sacramento Pass Basin, east-central Nevada; implications for the evolution of extensional detachment faults in the Basin and Range. Bull. Am. Assoc. Petrol. Geol. 83, 1891.

Martinez, C.M., Miller, E.L., Stockli, D.F., 1998. Miocene age rock avalanche deposits of the Sacramento Pass Basin, Basin and Range Province, Nevada. Geo. Soc. Am. Abstr. Programs vol. 30, pp. 53.

Miller, E.L., Gans, P.B., Grier, S.P., 1995. Geologic map of the Windy Peak 7.5' quadrangle, White Pine County, Nevada. U.S. Geol. Surv. Open File Map OF 94-0687 -.

Miller, E.L., Dumitru, T.A., Brown, R.W., Gans, P.B., 1999a. Rapid Miocene slip on the Snake Range-Deep Creek Range fault system, east-central Nevada. Geol. Soc. Am. Bull. 111, 886–905.

Miller, E.L., Gans, P.B., Grier, S.P., Huggins, C.C., Lee, J., 1999b. Preliminary Geologic Map of the Old Mans Canyon 7.5' Quadrangle, Northern Snake Range, White Pine County, Nevada. Nevada Bur. Mines Geol. Field Studies Map.

Mix, H., Mulch, A., Chamberlain, C.P., 2011. Cenozoic migration of topography in the North American Cordillera. Geology, 87–90, http://dx.doi.org/10.1130/G31450.1.

Molnar, P., Chen, W.P., 1983. Focal depths and fault plane solutions of earthquakes under the Tibetan Plateau. J. Geophys. Res. 88, 1180–1196.

Molnar, P., England, P., 1990. Late Cenozoic uplift of mountain ranges and global climate change: chicken or egg? Nature 346, 29–34.

Morrison, J., Anderson, J.L., 1998. Footwall refrigeration along a detachment fault: implications for the thermal evolution of core complexes. Science 279, 63–66.

Mulch, A., Chamberlain, C.P., 2007. Stable isotope paleoaltimetry in orogenic belts—the silicate record in surface and crustal geological archives. Rev. Mineral. Geochem. 66, 89–118.

Mulch, A., Graham, S.A., Chamberlain, C.P., 2006. Hydrogen isotopes in Eocene River gravels and paleoelevation of the Sierra Nevada. Science 313, 87–89.

Mulch, A., Teyssier, C., Cosca, M.A., Vanderhaeghe, O., Vennemann, T., 2004. Reconstructing paleoelevation in eroded orogens. Geology 32, 525–528.

Mulch, A., Teyssier, C., Chamberlain, C.P., Cosca, M.A., 2007. Stable isotope paleoaltimetry of Eocene core complexes in the North American Cordillera. Tectonics 26, 1–13, http://dx.doi.org/10.1029/2006TC001995.

Mulch, A., Sarna-Wojcicki, M., Perkins, M.E., Chamberlain, C.P., 2008. A Miocene to Pleistocene climate and elevation record of the Sierra Nevada (California). Proc. Natl. Acad. Sci. 105, 1–6.

Parrish, R.R., Carr, S.D., Parkinson, D.L., 1988. Eocene extensional tectonics and geochronology of the southern Omineca belt, British-Columbia and Washington. Tectonics 7, 181–212.

Poage, M.A., Chamberlain, C.P., 2001. Empirical relationships between elevation and the stable isotope composition of precipitation and surface waters: considerations for studies of paleoelevation change. Am. J. Sci. 301, 1–15.

Poage, M.A., Chamberlain, C.P., 2002. Stable isotopic evidence for a Pre-Middle Miocene rainshadow in the western Great Basin and Range: implications for the surface uplift of the Sierra Nevada. Tectonics 21, 16,1–16,10.

Poulsen, C.J., Jeffery, M.L., 2011. Climate change imprinting on stable isotopic compositions of high-elevation meteoric water cloaks past surface elevations of major orogens. Geology 39, 595–598.

Quade, J., Garzione, C., Eiler, J., 2007. Paleoelevation reconstruction using pedogenic carbonates. In: Kohn, M.J. (Eds.), Paleoaltimetry: Geochemical and Thermodynamic Approaches. Rev. Mineral. Geochem. 66, 53–88.

Quade, J., Breecker, D.O., Daëron, M., Eiler, J., 2011. The paleoaltimetry of Tibet: an isotopic perspective. Am. J. Sci. 311, 77–115, http://dx.doi.org/10.2475/02.2011.01.

Richard, S.M., Fryxell, J.E., Sutter, J.F., 1990. Tertiary structure and thermal history of the Harquahala and Buckskin Mountains, west central Arizona: implications for denudation by a major detachment fault system. J. Geophys. Res. 95, 19973–19987.

Rowley, D.B., Currie, B.S., 2006. Palaeo-altimetry of the late Eocene to Miocene Lunpola Basin, central Tibet. Nature 439, 677–681.

Rowley, D.B., Garzione, C.N., 2007. Stable isotope-based paleoaltimetry. Annu. Rev. Earth Planet. Sci. 35, 463–508.

Rozanski, K., Araguas-Araguas, L., Gonfiantini, R., 1993. Isotopic patterns in modern global precipitation. In: Swart, P.K., Lohmann, K.C., McKenzie, J., Savin, S. (Eds.), Climate Change in Continental Isotopic Records, 78. American Geophysical Union, Geophys. Monogr., Washington D.C., pp. 1–37.

Ruddiman, W.F., Kutzbach, J.E., 1989. Forcing of late Cenozoic Northern Hemisphere climate by plateau uplift in southern Asia and the American west. J. Geophys. Res. 94, 18409–18427.

Scott, R.J., Foster, D.A., Lister, G.S., 1998. Tectonic implications of rapid cooling of lower plate rocks from the Buckskin-Rawhide metamorphic core complex, west-central Arizona. Geol. Soc. Am. Bull. 110, 588–614.

Siegenthaler, U., Oeschger, H., 1980. Correlation of 18O in precipitation with temperature and altitude. Nature 285, 314–317.

Sonder, L.J., England, P.C., Wernicke, B.P., Christensen, R.L., 1987. A physical model for Cenozoic extension of western North America. In: Coward, M.P., Dewey, J.F., Hancock, P.L. (Eds.), Continental Extension Tectonics, 28. Geol. Soc. Spec. Publ. London, Oxford, UK, pp. 187–201.

Spencer, J.E., Reynolds, S.J., 1989. Tertiary structure, stratigraphy and tectonics of the Buckskin Mountains. In: Spencer, J.E., Reynolds, S.J. (Eds.), Geology and Mineral Resources of the Buckskin and Rawhide Mountains, West-central Arizona. Ariz. Geol. Surv. Bull., 198; 1989, pp. 103–167.

Spencer, J.E., Reynolds, S.J., 1991. Tectonics of mid-Tertiary extension along a transect through west-central Arizona. Tectonics 10, 1204–1221.

Suzuoki, T., Epstein, S., 1976. Hydrogen isotope fractionation between OH-bearing minerals and water. Geochim. Cosmochim. Acta 40, 1229–1240.

Teyssier, C., Ferré, E.C., Whitney, D.L., Norlander, B., Vanderhaeghe, O., Parkinson, D., 2005. Flow of partially molten crust and origin of detachments during collapse of the Cordilleran Orogen. Geol. Soc. Spec. Publ. London 245, 39–64.

Vanderhaeghe, O., Teyssier, C., McDougall, I., Dunlap, W.J., 2003. Cooling and exhumation of the Shuswap Metamorphic Core Complex constrained by $^{40}Ar/^{39}$ thermochronology. Geol. Soc. Am. Bull. 115, 200–216.

Wernicke, B., 1981. Low-angle normal faults in the Basin and Range Province: nappe tectonics in an extending orogeny. Nature 291, 645–648.

Wernicke, B. 1990. The fluid crustal layer and its implications for continental dynamics. In: Salisbury, M.H., Fountain, D.M. (Eds.), Exposed Cross-Sections of the Continental Crust. NATO ASI Series. Series C. Mathem. and Phys. Sciences vol. 317, pp. 509–544.

Wolfe, J.A., Schorn, H.E., Forest, C.E., Molnar, P., 1997. Paleobotanical evidence for high altitudes in Nevada during the Miocene. Science 276, 1672–1675.

Wright, J.E., Anderson, J.L., Davis, G.A., 1986. Timing of plutonism, mylonitization and decompression in a metamorphic core complex, Whipple Mountains, California. Geol. Soc. Am. Abst. Prog. 18, 201.